

Nodeless s -Wave Superconducting Phases in Cuprates with Ba_2CuO_3 -Type Structure

Zhi-Qiang Gao,^{1,*} Kai-Wei Sun,^{1,*} and Fa Wang^{1,2}

¹International Center for Quantum Materials, School of Physics, Peking University, Beijing 100871, China

²Collaborative Innovation Center of Quantum Matter, Beijing 100871, China

(Dated: October 19, 2021)

In this work zero-temperature phase diagrams of cuprates with Ba_2CuO_3 -type CuO chain structure is investigated. The projective symmetry group analysis is employed in the strong coupling limit, and renormalization group with bosonization analysis is employed in the weak coupling limit. We find that in both of these two limits, large areas of the phase diagrams are filled with nodeless s -wave superconducting phases (with weak d -wave components), instead of pure d -wave phase mostly found in cuprates. This implies that nodeless s -wave phase is the dominant superconducting phase in cuprates with Ba_2CuO_3 -type CuO chain structure in low temperature. Other phases are also found, including $(s + d)$ -wave superconducting phases and Luttinger liquid phases.

I. INTRODUCTION

CuO_2 plane^{1,2} plays an important role in the cuprate superconductors with high transition temperature (high- T_C)³⁻⁵, especially in the formation of d -wave pairing symmetry⁶⁻⁹. Traditionally, oxygen vacancies in CuO_2 planes are detrimental¹⁰ to high- T_C . However, recent experiments^{11,12} reported that in one kind of cuprates with a large amount of oxygen vacancies, $\text{Ba}_2\text{CuO}_{3+\delta}$ with $0 \leq \delta \leq 1$, high- T_C superconductivity is still observed. Various theoretical works^{11,13-18} focusing on $\text{Ba}_2\text{CuO}_{3+\delta}$ have been proposed to determine the pairing symmetry and low-temperature phases in different crystal structures. Liu¹⁹ and coworkers showed by first principle calculation that $\text{Ba}_2\text{CuO}_{3+\delta}$ can be viewed as doped Ba_2CuO_3 , which exhibits a CuO chain structure shown in Fig. 1 with one E_g orbital ($\text{Cu } 3d_{z^2-x^2}$) active, and with strong intra-chain and weak inter-chain anti-ferromagnetic (AFM) coupling. In this work, we study the zero-temperature phases in $\text{Ba}_2\text{CuO}_{3+\delta}$ by investigating a single-orbital multi-chain t-J model in both strong and weak coupling limits.

In both limits, we find that large areas of these phase diagrams are filled with s -wave superconducting phases (with weak d -wave components). It is s_{\pm} -wave with weak d -wave components (denoted as s_{\pm}^d -wave) in strong coupling limit, and s -wave with weak d -wave components (denoted as s_d -wave) in weak coupling limit. Both of them are nodeless on Fermi surfaces. This result indicates that the dominant superconducting phase in cuprates with Ba_2CuO_3 -type CuO chain structure in low temperature is actually a nodeless s -wave phase, in contrast to the traditional d -wave phase in cuprates with CuO_2 plane structure. This paper is organized as following. In Sec. II the single-orbital¹⁹ t-J model is introduced to describe the system. In Sec. III and IV, the strong and weak coupling limits are investigated and corresponding phase diagrams are given, respectively. We draw the conclusions in Sec. V. Details are listed in Appendix.

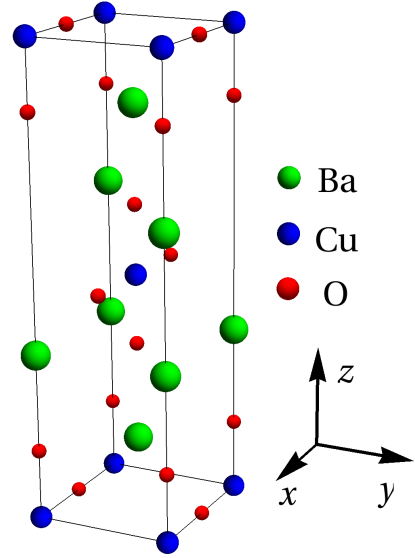


FIG. 1. The energetic preferred crystal structure¹⁹ of Ba_2CuO_3 .

II. THE MODEL

As indicated in Ref.¹⁹, the only active orbital is $\text{Cu } 3d_{z^2-x^2}$. Therefore, a single-orbital multi-chain t-J model is employed to describe the system. The Hamiltonian $H = H_0 + H'$ reads

$$\begin{aligned}
 H_0 = \sum_{x,y,z,s} & -t(c_{x,y,z,s}^\dagger c_{x+1,y,z,s} + h.c.) \\
 & -t_y(c_{x,y,z,s}^\dagger c_{x,y+1,z,s} + h.c.) \\
 & -t'(c_{x,y,z,s}^\dagger c_{x,y,z+1,s} + c_{x,y,z,s}^\dagger c_{x-1,y-1,z+1,s} \\
 & + c_{x,y,z,s}^\dagger c_{x-1,y,z+1,s} + c_{x,y,z,s}^\dagger c_{x,y-1,z+1,s} \\
 & + h.c.), \quad (1)
 \end{aligned}$$

and

$$\begin{aligned}
H' = & \sum_{x,y,z} J \vec{S}_{x,y,z} \cdot \vec{S}_{x+1,y,z} \\
& + J_y \vec{S}_{x,y,z} \cdot \vec{S}_{x,y+1,z} \\
& + J' \vec{S}_{x,y,z} \cdot (\vec{S}_{x,y,z+1} + \vec{S}_{x-1,y,z+1} \\
& + \vec{S}_{x,y-1,z+1} + \vec{S}_{x-1,y-1,z+1}), \quad (2)
\end{aligned}$$

where c 's (c^\dagger 's) are annihilation (creation) operators of electrons, parameters t, t_y, t_z, t' are hopping amplitudes with t largest¹⁹, J, J_y, J' are AFM couplings with J largest¹⁹, and $\vec{S}_{x,y,z} = \sum_{s,s'} c_{x,y,z,s}^\dagger \vec{\sigma}_{ss'} c_{x,y,z,s'}$ with x, y, z defined in Fig. 2 and Pauli matrices $\vec{\sigma} = (\sigma^1, \sigma^2, \sigma^3)$. Hopping and interaction on bonds perpendicular to xy -plane are neglected because of the large length^{11,19} of these bonds.

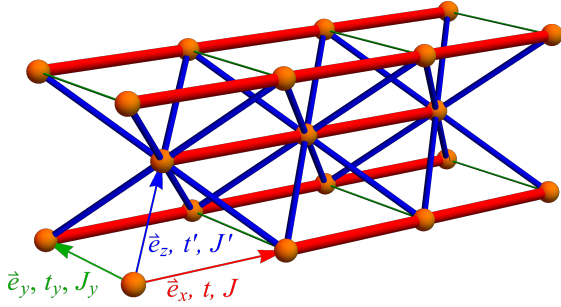


FIG. 2. The lattice of Ba_2CuO_3 . The x, y and z direction are defined in the figure. t, J are on the thickest red bonds, t', J' are on the mid-thick blue bonds, and t_y, J_y are on the thinnest green bonds.

In following sections, the single-orbital multi-chain t - J model (Eq. 1 and 2) is studied in strong and weak coupling limits.

III. STRONG COUPLING LIMIT

In the strong coupling limit ($t \ll J$), projective construction (slave particle) mean field approach²⁰⁻²² is employed to analyze possible phases. The mean field Hamiltonian is obtained for doping description through the $SU(2)$ slave boson approach²². These phases are characterized by mean field ansatzes classified by projective symmetry groups²⁰⁻²² (PSG's). Numerical minimization of mean field energy is employed to determine the phase diagram.

A. Mean Field Hamiltonian

A variation method is used in this section to analyze phases. A series of mean field ansatzes are introduced representing different situations of ground states

and are further optimized utilizing differential evolution algorithm.

In this approach operators of electrons are represented in spin-0 charged bosons (holons) $b_i = (b_{1,i}, b_{2,i})^T$ and spin-1/2 neutral fermions (spinons) $\psi_i = (f_{\uparrow,i}, f_{\downarrow,i})^T$ via²²

$$c_{\uparrow,i} = \frac{1}{\sqrt{2}} b_i^\dagger \psi_i, \quad (3)$$

$$c_{\downarrow,i} = \frac{1}{\sqrt{2}} b_i^\dagger \bar{\psi}_i, \quad (4)$$

where $\bar{\psi}_i = (f_{\downarrow,i}, -f_{\uparrow,i})^T$. In this representation, the mean field Hamiltonian reads²²

$$\begin{aligned}
H_{\text{MF}} = & \frac{3}{4} \sum_{\langle ij \rangle} J_{ij} (\text{tr}(u_{ij}^\dagger u_{ij}) + (\psi_i^\dagger u_{ij} \psi_j + h.c.)) \\
& - \sum_{\langle ij \rangle} t_{ij} (b_i^\dagger u_{ij} b_j + h.c.) \quad (5)
\end{aligned}$$

where J 's and t 's are determined by Eq. 1 and Eq. 2, u_{ij} is the mean field ansatz²²

$$u_{ij} = \delta_{\alpha\beta} \begin{pmatrix} -\langle f_{i,\alpha}^\dagger f_{j,\beta} \rangle^* & \langle f_{i,\alpha} f_{j,\beta} \rangle \\ \langle f_{i,\alpha} f_{j,\beta} \rangle^* & \langle f_{i,\alpha}^\dagger f_{j,\beta} \rangle \end{pmatrix}. \quad (6)$$

There are two kinds of constraints²², namely proper filling

$$\langle b_i^\dagger b_i \rangle = 2\delta \quad (7)$$

and physical states

$$\langle \psi_i^\dagger \tau^l \psi_i + b_i^\dagger \tau^l b_i \rangle = 0, \quad l = 1, 2, 3. \quad (8)$$

where τ 's are Pauli matrices. To implement these constraints, an additional penalty term should be added to the original Hamiltonian:

$$\begin{aligned}
H_{\text{penalty}} = & \sum_{i,l} P(\langle \psi_i^\dagger \tau^l \psi_i + b_i^\dagger \tau^l b_i \rangle) \\
& - P(\sum_i \langle b_i^\dagger b_i \rangle - 2\delta), \quad (9)
\end{aligned}$$

where $P(x)$ is a penalty function, $P(x) = Gx^2$ with G being huge (larger than 10^9 in practice). In the determination of mean field ansatzes, it is required that $P(x)$ does not contribute to mean field energy in final solutions found.

B. Projective Symmetry Groups Analysis and Schematic Phase Diagram

Different phases characterized by mean field ansatzes of different kinds of Z_2 spin liquid are classified by PSG's²⁰. The PSG's compose certain constraints on ansatzes, and at most 311 gauge inequivalent ansatzes are

found. Details are presented in Appendix A. To further determine the phase diagram, the differential evolution algorithm is employed. With constraints from PSG's, number of optimizing variables are restricted to be 12, so that this global optimizing algorithm is sufficient.

J'/J and filling δ are used as variables of the phase diagram. In what follows, the phase diagram is calculated in the case $t = 2t' = 2t_y = 0.02J$ and $J_y = 0.5J$. This set of coefficients satisfies that inter-chain hopping and coupling are smaller than intra-chain ones¹⁹. The practical calculation is performed on a $16 \times 16 \times 16$ lattice with periodic boundary condition. For numerical details refer to Appendix B. With 25 choices of parameters investigated, the schematic phase diagram is obtained, as shown in Fig. 3. However, in region $J'/J < 0.5, \delta < 0.1$, the numerical results are not reliable. This region of phase diagram is left blank.

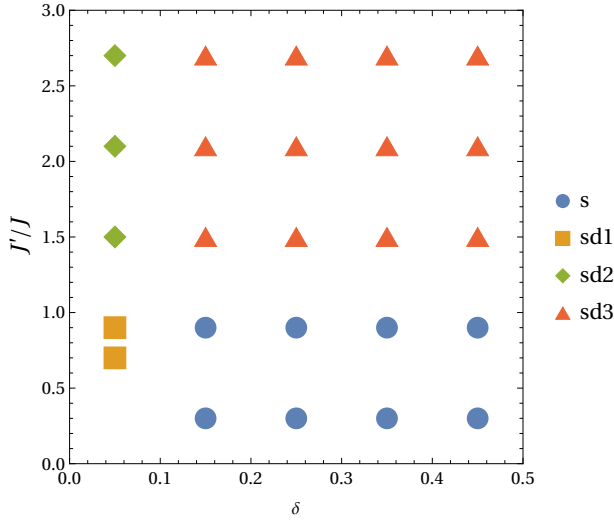


FIG. 3. Schematic phase diagram in strong coupling limit with $t = 2t' = 2t_y = 0.04J_y = 0.02J$. "s" and "sd" means s_{\pm}^d -wave and $(s + d)$ -wave superconductivity, respectively. The bottom left corner of the phase diagram is left blank since numerical results are not reliable in this region.

In the region of coefficients we choose, there are 4 phases in total. At zero temperature, the holons necessarily condense, and the system is consequently in superconducting phases.

(i) The s_{\pm}^d -wave superconducting phase, namely s_{\pm} -wave with weak d -wave components, shown as "s" in Fig. 3, described by

$$\begin{aligned} u_{i,i+\hat{x}} &= \Delta_x \tau^1 - \chi_x \tau^3, \\ u_{i,i+\hat{y}} &= \Delta_y \tau^1 - \chi_y \tau^3, \\ u_{i,i+\hat{z}} &= u_{i,i+\hat{z}-\hat{x}} = u_{i,i+\hat{z}-\hat{y}} = u_{i,i+\hat{z}-\hat{x}-\hat{y}} \\ &= \Delta_z \tau^1 - \chi_z \tau^3 + i\chi'_z \tau^0. \end{aligned} \quad (10)$$

Unlike what discussed in Ref.²⁰, due to the absence of 4-fold rotation symmetry, weak d -wave components inevitably coexist in the s -wave superconducting phase. However, if the system exhibits s -wave superconductivity

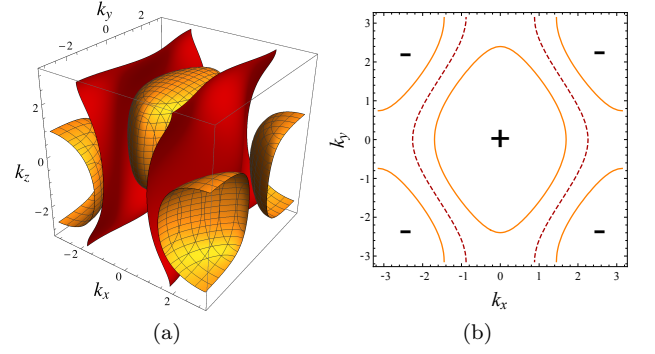


FIG. 4. (a) Fermi surfaces shown by yellow meshed surfaces and zeros of superconducting gap shown by red meshless surfaces in s_{\pm}^d -wave phase. (b) The projection to $k_z = 0$ plane, where Fermi surfaces are shown by yellow solid curves and zeros of superconducting gap are shown by red dashed curve. The sign of superconducting gap on Fermi surfaces are shown as "+" and "-". Here $\delta = 0.25$.

in general, it is still considered as an s -wave phase. The spinon Fermi surfaces and the zeros of superconducting gap of the s_{\pm}^d -wave phase we find are shown in Fig. 4. Since holons condense in this phase, the spinon Fermi surfaces are the same as the electron Fermi surfaces. The superconducting gap on the Fermi surfaces has no node, which corroborates that in this phase s_{\pm} -wave pairing is dominant.

(ii) The first $(s + d)$ -wave superconducting phase, shown as "sd1" in Fig. 3, described by

$$\begin{aligned} u_{i,i+\hat{x}} &= \Delta_x \tau^1 - \chi_x \tau^3, \\ u_{i,i+\hat{y}} &= \Delta_y \tau^1 + \chi_y \tau^3, \\ u_{i,i+\hat{z}} &= u_{i,i+\hat{z}-\hat{x}} = u_{i,i+\hat{z}-\hat{y}} = u_{i,i+\hat{z}-\hat{x}-\hat{y}} \\ &= -\Delta_z \tau^1 - \chi_z \tau^3. \end{aligned} \quad (11)$$

(iii) The second $(s + d)$ -wave superconducting phase, shown as "sd2" in Fig. 3, described by

$$\begin{aligned} u_{i,i+\hat{x}} &= \Delta_x \tau^1 - \chi_x \tau^3, \\ u_{i,i+\hat{y}} &= \Delta_y \tau^1 - \chi_y \tau^3, \\ u_{i,i+\hat{z}} &= -u_{i,i+\hat{z}-\hat{x}} = u_{i,i+\hat{z}-\hat{y}} = u_{i,i+\hat{z}-\hat{x}-\hat{y}} \\ &= \Delta_z \tau^1 - i\chi'_z \tau^0. \end{aligned} \quad (12)$$

(iv) The third $(s + d)$ -wave superconducting phase, shown as "sd3" in Fig. 3, described by

$$\begin{aligned} u_{i,i+\hat{x}} &= \Delta_x \tau^1 - \chi_x \tau^3, \\ u_{i,i+\hat{y}} &= \Delta_y \tau^1 - \chi_y \tau^3, \\ u_{i,i+\hat{z}} &= -u_{i,i+\hat{z}-\hat{x}} = u_{i,i+\hat{z}-\hat{y}} = u_{i,i+\hat{z}-\hat{x}-\hat{y}} \\ &= \Delta_z \tau^1 - \chi_z \tau^3 - i\chi'_z \tau^0. \end{aligned} \quad (13)$$

As a comparison, we also find that the superconducting gap has nodes on Fermi surfaces in $(s + d)$ -wave phases. All of the four ansatzes are consistent with the PSG analysis.

In conclusion, in strong coupling limit, the phase diagram is largely filled with the nodeless s_{\pm}^d -wave superconducting phase in the physical relevant regime of coefficients ($J'/J < 1$).

IV. WEAK COUPLING LIMIT

In the weak coupling limit ($t \gg J$), renormalization group (RG) and bosonization analysis are employed to determine possible phases.

A. Quasi-1D Model

An $N = 2$ chains²³ model is considered, as shown in Fig. 5. Some previous work have focused on Luttinger liquids on two-leg ladders with^{24–26} or without frustration^{23,27–34}. However, the lattice structure in this model has not been investigated. Since the intra-chain coupling plays a more important role than that of the inter-chain coupling¹⁹, and the translation symmetries of the conventional unit cells are presumably not destroyed, this quasi-1D model is believed to capture the most relevant physics. The unit cell is changed to be the conventional unit cell with two atoms in one unit cell, and the z direction is redefined. In the redefined coordinate, the

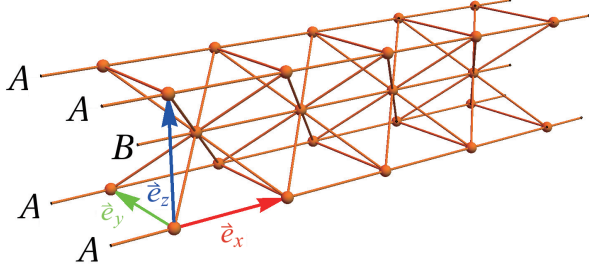


FIG. 5. The $N = 2$ chains model. Here four A chains are equivalent under periodic boundary condition, while B chain is inequivalent to them. The unit cell is modified to be the conventional unit cell with two inequivalent atoms in one unit cell, and the z direction is redefined.

non-interacting Hamiltonian H_0 can be diagonalized as

$$H_0 = \sum_{\vec{k}, s; i=1,2} \epsilon_i(\vec{k}) \psi_{i,s}^\dagger(\vec{k}) \psi_{i,s}(\vec{k}), \quad (14)$$

where

$$\begin{aligned} \epsilon_{1,2}(\vec{k}) = & -2(\pm t'(\cos(k_x + k_y + \frac{k_z}{2}) + \cos(k_x - k_y + \frac{k_z}{2})) \\ & + \cos(-k_x + k_y + \frac{k_z}{2}) + \cos(k_x - k_y - \frac{k_z}{2})) \\ & + t \cos(k_x) + t_y \cos(k_y), \end{aligned} \quad (15)$$

where $+$ ($-$) sign for $\epsilon_{1(2)}$, respectively. For the $N = 2$ chains model, the summation over \vec{k} only contains those points with $k_y = k_z = 0$. Therefore, the Fermi points are determined via²³

$$\epsilon_i(k_{Fi}) = \mu, \quad i = 1, 2, \quad (16)$$

for chemical potential μ . The Fermi points in this quasi-1D model can be viewed as a discrete set of points with $k_y = k_z = 0$ on the 3D Fermi surface of the $N = +\infty$ model. As shown in Fig. 6. For clarity the k_y direction is neglected. For a generic filling, the Fermi points does not coincide, and there is no umklapp interactions.

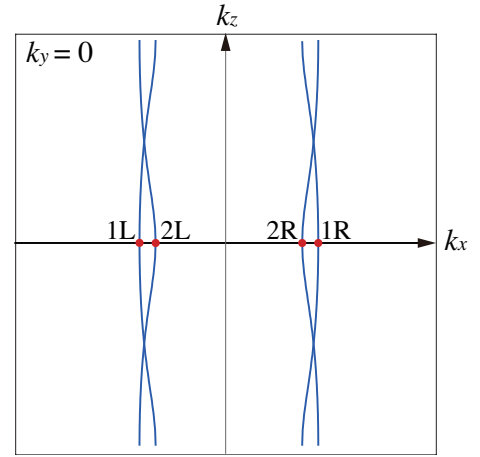


FIG. 6. The Fermi points named 1L, 1R and 2L, 2R as the intersection of the Fermi surfaces (blue curves) and line $k_y = k_z = 0$. Here $\delta = 0.2$.

Only excitations around Fermi points are considered in long wave length limit. Field operators can be written in terms of chiral fermions (right/left movers) as²³

$$\psi_{i,s} \sim \psi_{i,s}^R e^{ik_{Fi}x} + \psi_{i,s}^L e^{-ik_{Fi}x}, \quad i = 1, 2, \quad (17)$$

with $\psi_{1,s}^L$, $\psi_{1,s}^R$, $\psi_{2,s}^L$ and $\psi_{2,s}^R$ corresponding to excitation around Fermi point 1L, 1R, 2L and 2R, respectively. The momenta of these chiral fermions are bounded by a momentum cut-off $\Lambda \ll k_{F1,2}$. Therefore, the dispersion can be linearized within Λ . The effective non-interacting Hamiltonian reads

$$H_0 = \sum_{i,s} \int dx v_i (\psi_{i,s}^{R\dagger} i \partial_x \psi_{i,s}^R - \psi_{i,s}^{L\dagger} i \partial_x \psi_{i,s}^L), \quad (18)$$

where $v_i = \partial_{k_x} \epsilon_i(\vec{k})|_{k_x=k_{Fi}, k_y=k_z=0}$ is the Fermi velocity.

B. Renormalization Group and Bosonization Analysis

A generic interaction Hamiltonian density subject to the constraint of momenta conservation reads

$$\begin{aligned} \mathcal{H}' = & \sum_{i,j=1}^2 f_{ij}^{\rho} T_{ii}^R T_{jj}^L - f_{ij}^{\sigma} \vec{T}_{ii}^R \cdot \vec{T}_{jj}^L \\ & + \sum_{i=1}^2 f_{ii}^{\rho} T_{i,3-i}^R T_{i,3-i}^L - f_{i,i}^{\sigma} \vec{T}_{i,3-i}^R \cdot \vec{T}_{i,3-i}^L, \end{aligned} \quad (19)$$

where currents

$$T_{ij} = \sum_s \psi_{i,s}^{\dagger} \psi_{j,s}, \quad (20)$$

$$\vec{T}_{ij} = \frac{1}{2} \sum_{s,s'} \psi_{i,s}^{\dagger} \vec{\sigma}_{ss'} \psi_{j,s'}. \quad (21)$$

Coupling constants f 's and (f') 's represent intra-band and inter-band scattering, respectively. The relationship of their values are given by certain symmetries. Charge conjugation $T_{ij} \rightarrow T_{ji}$ gives $f'_{ii} = f'_{3-i,3-i}$, while reflection in x direction gives²³ $f_{ij} = f_{ji}$. Details of the construction of this interaction Hamiltonian density is left in Appendix C.

To construct a low energy effective theory, the interaction is renormalized and bosonized. The derivation of the RG equations is left in Appendix D. After solving RG equations numerically, in the region of coefficients adopted, we find that in all cases there are two coupling constants, $(f_{11}^{\rho}, f_{11}^{\sigma})$ or $(f_{22}^{\rho}, f_{22}^{\sigma})$, dominant. Since f^{ρ} only contribute gradient term after bosonization²³, they are simply dropped. Therefore, the interaction Hamiltonian after RG reads (take subscript 1 as example)

$$\mathcal{H}' = \sum_s \frac{1}{2} f_{11}^{\sigma} \psi_{1,s}^{R\dagger} \psi_{1,\bar{s}}^{L\dagger} \psi_{1,\bar{s}}^L \psi_{1,s}^R, \quad (22)$$

where \bar{s} means the opposite direction of spin s . After bosonization, in terms of the chiral boson fields, the Hamiltonian reads (take subscript 1 as an example)

$$\mathcal{H}_0 \sim \frac{v_1}{2} ((\partial_x \theta_{1,\sigma})^2 + (\partial_{\tau} \theta_{1,\sigma})^2), \quad (23)$$

$$\mathcal{H}' \sim f_{11}^{\sigma} \cos(\sqrt{8\pi} \theta_{1,\sigma}), \quad (24)$$

Purely free fields are neglected in \mathcal{H}_0 . Therefore, the low energy effective theory of the system is a sine-Gordon theory. The bosonization dictionary is left in Appendix E, including the definition of $\theta_{i,\sigma}$.

C. Phase Diagram

The global minima of Eq. 24 is

$$\sqrt{2\pi} \theta_{i,\sigma} = 2l_i \pi \quad \text{or} \quad (2l_i + 1)\pi, \quad l_i \in \mathbb{Z}, \quad (25)$$

depending on the sign of f_{ii}^{σ} . Around a minimum, the interaction Hamiltonian can be expanded as $\mathcal{H}' \sim m(\delta\theta)^2$,

which gives the field θ an effective mass. Therefore, when one f^{σ} is dominant, there is one gapless spin mode and one gapped spin mode. The two charge modes are always gapless. To figure out the phase diagrams, the expectation values of different order parameters are calculated, including charge density wave (CDW), spin density wave (SDW), singlet superconductivity (SS) and triplet superconductivity (TS):³⁵

$$\mathcal{O}_{\text{CDW},i} = \sum_s \psi_{i,s}^{R\dagger}(x) \psi_{i,s}^L(0), \quad (26)$$

$$\vec{\mathcal{O}}_{\text{SDW},i} = \sum_{s,s'} \psi_{i,s}^{R\dagger}(x) \vec{\sigma}_{ss'} \psi_{i,s'}^L(0), \quad (27)$$

$$\mathcal{O}_{\text{SS},i} = \psi_{i,\uparrow}^{R\dagger}(x) \psi_{i,\downarrow}^{L\dagger}(0), \quad (28)$$

$$\mathcal{O}_{\text{TS},i} = \psi_{i,\uparrow}^{R\dagger}(x) \psi_{i,\uparrow}^{L\dagger}(0). \quad (29)$$

These order parameters can be rewritten in terms of boson fields via the bosonization dictionary in Appendix E. As indicated in Ref.²³, according to the uncertainty principle $[\phi, \theta] = O(1)$, the conjugate field of θ_{σ} , namely ϕ_{σ} , fluctuates violently. Therefore, only terms like $e^{i\phi_{\sigma}(x) - \phi_{\sigma}(0)}$ can survive in the mean field level. Applying this criteria, one can determine whether the order parameters are non-vanishing in certain phases.

Without losing generality, f_{11}^{σ} is supposed to be dominant. All the non-vanishing order parameters are \mathcal{O}_{CDW} , $\vec{\mathcal{O}}_{\text{SDW}}$ and \mathcal{O}_{SS} . When f_{11}^{σ} is negative, according to the Cooper instability, an attractive interaction will naturally induce superconductivity. Therefore, the system will be in an s -wave superconducting phase (with weak d -wave components due to the absence of four-fold rotation symmetry). When f_{11}^{σ} is positive, both CDW and SDW can exist in this system, due to the gaplessness of the charge modes and the spin mode. The system will present spin-charge separation and hence in a Luttinger liquid phase with two gapless charge modes and one gapless spin mode.

The phase diagram is shown in Fig. 7. We use t'/t and filling δ as variables, and fix other coefficients as $t_y = 0.5t$ and $J = 3J' = 6J_y = 0.03t$ to satisfy that inter-chain hopping and coupling are smaller than intra-chain ones¹⁹. The phase diagram is largely occupied by s -wave superconducting phase with weak d -wave components (denoted as s_d -wave in Fig. 7). For appropriate filling, one of the two bands is fully empty or fully occupied, leading to only two Fermi points, instead of four, participating in interactions. In this case, the only dominant coupling constants are f^{ρ} 's, implying all of the two charge modes and two spin modes are gapless in this Luttinger liquid phase denoted as²³ "C2S2" in Fig. 7. The other Luttinger liquid phase with two gapless charge modes and one spin mode is denoted as²³ "C2S1". In the s_d -wave phase, the pairing order parameter has no node in k -space, since the mean field decomposition of interaction Hamiltonian density Eq. 22 can be rearranged into the form of a traditional BCS Hamiltonian. Therefore, the superconducting gap has the same sign on all the four

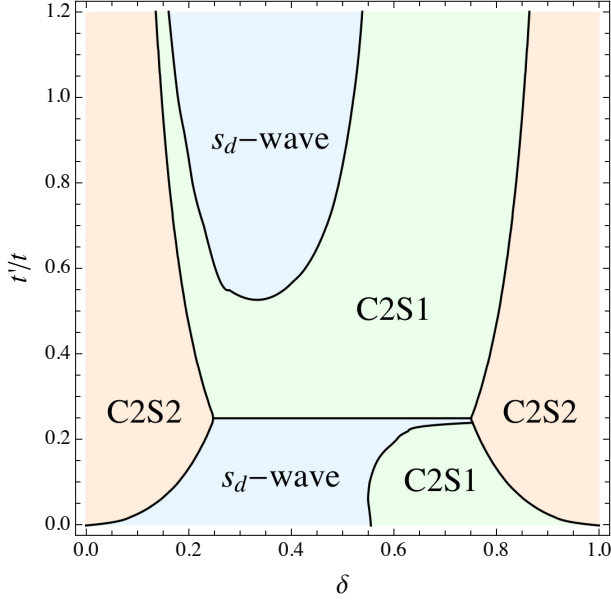


FIG. 7. Phase diagram in weak coupling limit with $J = 3J' = 6J_y = 0.06t_y = 0.03t$. "CmSn" stands for Luttinger liquid phase with m gapless charge modes and n gapless spin modes²³. " s_d -wave" stands for s -wave superconducting phase with weak d -wave components.

Fermi points, 1L, 1R and 2L, 2R. The superconducting phase is therefore a nodeless s_d -wave phase.

V. CONCLUSIONS

In this work zero-temperature phases of cuprates with $\text{Ba}_2\text{CuO}_{3+\delta}$ -type CuO chain structure are investigated in both strong and weak coupling limits of a single-orbital multi-chain t-J model. We find that in both of the two limits, the phase diagrams are largely filled with nodeless s -wave superconducting phases (with weak d -wave components). It is s_{\pm} -wave with weak d -wave components (denoted as s_{\pm}^d -wave) in strong coupling limit, and s -wave with weak d -wave components (denoted as s_d -wave) in weak coupling limit. We believe that our conclusion of nodeless s -wave pairing in $\text{Ba}_2\text{CuO}_{3+\delta}$ is consistent with the experimental observations of the stability of high- T_C against disorder^{11,36,37}. Some previous theories^{13,17} also proposed s_{\pm} -wave phases. However, they are based on multi-orbital models and developed on lattice structures apparently different from ours. d -wave superconductivity was also proposed in previous works^{14,15}. Our proposed nodeless s -wave pairing symmetry can in principle be detected in phase sensitive^{38,39} and spectroscopic⁴⁰ measurements.

VI. ACKNOWLEDGEMENT

ZQG and KWS acknowledge Hui Yang, Jie-Ran Xue and Xue-Mei Wang for enlightening discussions. FW acknowledges support from The National Key Research and Development Program of China (Grant No. 2017YFA0302904), and National Natural Science Foundation of China (Grant No. 11888101).

Appendix A: Classification of \mathbb{Z}_2 Spin Liquids Phases in $\text{Ba}_2\text{CuO}_{3+\delta}$

1. Projective Symmetry Groups

Under coordinates we choose in Sec. III, space group symmetries, including translation, parity, and inversion, read

$$T_x : (i_x, i_y, i_z) \mapsto (i_x + 1, i_y, i_z), \quad (\text{A1})$$

$$T_y : (i_x, i_y, i_z) \mapsto (i_x, i_y + 1, i_z), \quad (\text{A2})$$

$$T_z : (i_x, i_y, i_z) \mapsto (i_x, i_y, i_z + 1), \quad (\text{A3})$$

$$P_x : (i_x, i_y, i_z) \mapsto (-i_x - i_z, i_y, i_z), \quad (\text{A4})$$

$$P_y : (i_x, i_y, i_z) \mapsto (i_x, -i_y - i_z, i_z), \quad (\text{A5})$$

$$I : (i_x, i_y, i_z) \mapsto (-i_x, -i_y, -i_z), \quad (\text{A6})$$

and the time-reversal symmetry is

$$\mathcal{T} : u_{ij} \mapsto -u_{ij}. \quad (\text{A7})$$

The symmetries above satisfy equalities

$$T_x^{-1}T_y^{-1}T_xT_y = 1, \quad (\text{A8})$$

$$T_y^{-1}T_z^{-1}T_yT_z = 1, \quad (\text{A9})$$

$$T_z^{-1}T_x^{-1}T_zT_x = 1, \quad (\text{A10})$$

$$T_xP_xT_xP_x = 1, \quad (\text{A11})$$

$$T_yP_yT_yP_y = 1, \quad (\text{A12})$$

$$T_x^{-1}P_yT_xP_y = 1, \quad (\text{A13})$$

$$T_y^{-1}P_xT_yP_x = 1, \quad (\text{A14})$$

$$P_xT_xT_z^{-1}P_xT_z = 1, \quad (\text{A15})$$

$$P_yT_yT_z^{-1}P_yT_z = 1, \quad (\text{A16})$$

$$P_xP_yP_xP_y = 1, \quad (\text{A17})$$

$$P_x^2 = P_y^2 = 1, \quad (\text{A18})$$

$$T_xIT_xI = 1, \quad (\text{A19})$$

$$T_yIT_yI = 1, \quad (\text{A20})$$

$$T_zIT_zI = 1, \quad (\text{A21})$$

$$P_xIP_xI = 1, \quad (\text{A22})$$

$$P_yIP_yI = 1, \quad (\text{A23})$$

$$I^2 = 1. \quad (\text{A24})$$

\mathcal{T} commutes with all the space group symmetries. Following Ref²⁰, we can first determine G_x , G_y , G_z , and G_T

through Eq.A8, Eq.A9 Eq.A10 and the commutation relations between \mathcal{T} and translations. Unlike the 2D case²⁰, here we choose the gauge that

$$G_z(i) = \tau^0, \quad (\text{A25})$$

$$G_x(i) = \eta_x^{i_z} \tau^0, \quad (\text{A26})$$

$$G_y(i) = \eta_y^{i_z} \eta_{xy}^{i_x} \tau^0, \quad (\text{A27})$$

$$G_T(i) = g_T \eta_{xt}^{i_x} \eta_{yt}^{i_y} \eta_{zt}^{i_z}, \quad (\text{A28})$$

where two gauge inequivalent choices of g_T are $g_T = \tau^0$ or $i\tau^3$, and seven η s are ± 1 .

Then we consider parities P_x and P_y . The PSG equations given by Eq.A11 to Eq.A18 read

$$G_x(P_x(i))G_{P_x}^{-1}(i+\hat{x})G_x(i+\hat{x})G_{P_x}(i) \in \mathcal{G}, \quad (\text{A29})$$

$$G_y^{-1}(P_x(i))G_{P_x}^{-1}(i)G_y(i)G_{P_x}(i-\hat{y}) \in \mathcal{G}, \quad (\text{A30})$$

$$G_x^{-1}(P_y(i))G_{P_y}^{-1}(i)G_x(i)G_{P_y}(i-\hat{x}) \in \mathcal{G}, \quad (\text{A31})$$

$$G_y(P_y(i))G_{P_y}^{-1}(i+\hat{y})G_y(i+\hat{y})G_{P_y}(i) \in \mathcal{G}, \quad (\text{A32})$$

$$G_{P_x}(i)G_x(P_x(i))G_z^{-1}(T_z T_x^{-1} P_x(i)) \cdot$$

$$G_{P_x}(T_z T_x^{-1} P_x(i))G_z(T_z T_x^{-1}(i)) \in \mathcal{G}, \quad (\text{A33})$$

$$G_{P_y}(i)G_y(P_y(i))G_z^{-1}(T_z T_y^{-1} P_y(i)) \cdot$$

$$G_{P_y}(T_z T_y^{-1} P_y(i))G_z(T_z T_y^{-1}(i)) \in \mathcal{G}, \quad (\text{A34})$$

$$G_{P_x}(i)G_{P_y}(P_x(i))G_{P_x}^{-1}(P_y(i))G_{P_y}^{-1}(i) \in \mathcal{G}, \quad (\text{A35})$$

$$G_{P_x}(i)G_{P_x}(P_x(i)) \in \mathcal{G}, \quad (\text{A36})$$

$$G_{P_y}(i)G_{P_y}(P_y(i)) \in \mathcal{G}. \quad (\text{A37})$$

Since P_x and P_y do not change i_z , in our gauge Eq.A29 to Eq.A32 reduce to

$$G_{P_x}^{-1}(i+\hat{x})G_{P_x}(i) = \eta_{xpx} \tau^0, \quad (\text{A38})$$

$$G_{P_x}^{-1}(i+\hat{y})G_{P_x}(i) = \eta_{ypx} \eta_{xy}^{i_z} \tau^0, \quad (\text{A39})$$

$$G_{P_y}^{-1}(i+\hat{x})G_{P_y}(i) = \eta_{xpy} \tau^0, \quad (\text{A40})$$

$$G_{P_y}^{-1}(i+\hat{y})G_{P_y}(i) = \eta_{ypy} \tau^0, \quad (\text{A41})$$

which give $G_{P_x}(i)$ and $G_{P_y}(i)$ the generic form

$$G_{P_x}(i) = g_{P_x} \Theta_{P_x}(i_z) \eta_{xpx}^{i_x} \eta_{ypy}^{i_y}, \quad (\text{A42})$$

$$G_{P_y}(i) = g_{P_y} \Theta_{P_y}(i_z) \eta_{xpy}^{i_x} \eta_{ypy}^{i_y} \eta_{xy}^{i_z}, \quad (\text{A43})$$

where Θ s are (± 1) -valued functions of i_z . Eq.A33 to Eq.A37 then reduce to

$$g_{P_x}^2 \Theta_{P_x}(i_z) \Theta_{P_x}(i_z+1) \eta_{xpx}^{i_z+1} G_x(i) = \eta_{5px} \tau^0, \quad (\text{A44})$$

$$g_{P_y}^2 \Theta_{P_y}(i_z) \Theta_{P_y}(i_z+1) \eta_{xy}^{i_y} G_y(i) = \eta_{5py} \tau^0, \quad (\text{A45})$$

$$g_{P_x} g_{P_y} g_{P_x}^{-1} g_{P_y}^{-1} (\eta_{xpy} \eta_{ypr})^{i_z} = \pm \tau^0, \quad (\text{A46})$$

$$g_{P_x}^2 \eta_{xpx}^{i_z} = \pm \tau^0, \quad (\text{A47})$$

$$g_{P_y}^2 (\eta_{ypy} \eta_{xy})^{i_z} = \pm \tau^0, \quad (\text{A48})$$

for all sites i . Eq.A46 to Eq.A48 require that

$$\eta_{xpy} = \eta_{ypr}, \eta_{xy} = \eta_{xpx} = \eta_{ypy} = 1, \quad (\text{A49})$$

while Eq.A44 and Eq.A45 give two Θ s a specific form. All gauge inequivalent Θ s are

$$\Theta_{P_x}(i_z) = \eta_{5px}^{i_z}, \text{ for } G_x(i) = \tau^0; \quad (\text{A50})$$

$$\Theta_{P_y}(i_z) = \eta_{5py}^{i_z}, \text{ for } G_y(i) = \tau^0; \quad (\text{A51})$$

$$\Theta_{P_x}(i_z) = \eta_{5px}^{i_z} \cdot \sqrt{2} \sin(\frac{\pi}{2} i_z + \frac{\pi}{4}),$$

$$\text{for } G_x(i) = (-)^{i_z} \tau^0; \quad (\text{A52})$$

$$\Theta_{P_y}(i_z) = \eta_{5py}^{i_z} \cdot \sqrt{2} \sin(\frac{\pi}{2} i_z + \frac{\pi}{4}),$$

$$\text{for } G_y(i) = (-)^{i_z} \tau^0. \quad (\text{A53})$$

Finally we consider inversion I . Eq.A19 to Eq.A21 induce PSG equations

$$G_x(I(i))G_I(i+\hat{x})G_x(i+\hat{x})G_I(i) \in \mathcal{G}, \quad (\text{A54})$$

$$G_y(I(i))G_I(i+\hat{y})G_y(i+\hat{y})G_I(i) \in \mathcal{G}, \quad (\text{A55})$$

$$G_z(I(i))G_I(i+\hat{z})G_z(i+\hat{z})G_I(i) \in \mathcal{G}. \quad (\text{A56})$$

Under our gauge, $G_I(i)$ has the generic form

$$G_I(i) = g_I \eta_{xi}^{i_x} \eta_{yi}^{i_y} \eta_{zi}^{i_z}. \quad (\text{A57})$$

According to Eq.A22 and Eq.A23,

$$G_I(P_x(i))G_{P_x}^{-1}(I(i))G_x(I(i))G_{P_x}(i) \in \mathcal{G}, \quad (\text{A58})$$

$$G_I(P_y(i))G_{P_y}^{-1}(I(i))G_y(I(i))G_{P_y}(i) \in \mathcal{G}, \quad (\text{A59})$$

we have

$$g_I g_{P_x}^{-1} g_I g_{P_x} \eta_{xi}^{i_z} = \pm \tau^0, \quad (\text{A60})$$

$$g_I g_{P_y}^{-1} g_I g_{P_y} \eta_{yi}^{i_z} = \pm \tau^0, \quad (\text{A61})$$

for all sites i . Therefore, $\eta_{xi} = \eta_{yi} = 1$. From just the same argument, $\eta_{xt} = \eta_{yt} = 1$. Then, Eq.A28, Eq.A42, Eq.A43 and Eq.A57 reduce to

$$G_T(i) = g_T \eta_t^{i_z}, \quad (\text{A62})$$

$$G_{P_x}(i) = g_{P_x} \Theta_{P_x}(i_z) \eta_p^{i_y}, \quad (\text{A63})$$

$$G_{P_y}(i) = g_{P_y} \Theta_{P_y}(i_z) \eta_p^{i_x}, \quad (\text{A64})$$

$$G_I(i) = g_I \eta_I^{i_z}, \quad (\text{A65})$$

where η_t , η_p and η_I can take value of ± 1 , and $\Theta_{P_x}(i_z)$ and $\Theta_{P_y}(i_z)$ are determined above. The constraints of g s reduce to

$$g_{P_x}^2 = g_{P_y}^2 = g_I^2 = \pm \tau^0, \quad (\text{A66})$$

$$g_{P_x} g_{P_y} g_{P_x}^{-1} g_{P_y}^{-1} = \pm \tau^0, \quad (\text{A67})$$

$$g_I g_{P_x}^{-1} g_I g_{P_x} = \pm \tau^0, \quad (\text{A68})$$

$$g_I g_{P_y}^{-1} g_I g_{P_y} = \pm \tau^0, \quad (\text{A69})$$

$$g_T g_{P_x}^{-1} g_T g_{P_x} = \pm \tau^0, \quad (\text{A70})$$

$$g_T g_{P_y}^{-1} g_T g_{P_y} = \pm \tau^0, \quad (\text{A71})$$

$$g_I g_T^{-1} g_I g_T = \pm \tau^0. \quad (\text{A72})$$

All gauge inequivalent choices of g s are

$$g_T = \tau^0 \quad g_{P_x} = \tau^0 \quad g_{P_y} = \tau^0 \quad g_I = \tau^0; \quad (\text{A73})$$

$$g_T = \tau^0 \quad g_{P_x} = i\tau^3 \quad g_{P_y} = i\tau^3 \quad g_I = i\tau^3; \quad (\text{A74})$$

$$g_T = i\tau^3 \quad g_{P_x} = \tau^0 \quad g_{P_y} = \tau^0 \quad g_I = \tau^0; \quad (\text{A75})$$

$$g_T = i\tau^3 \quad g_{P_x} = i\tau^3 \quad g_{P_y} = i\tau^3 \quad g_I = i\tau^3; \quad (\text{A76})$$

$$g_T = i\tau^3 \quad g_{P_x} = i\tau^1 \quad g_{P_y} = i\tau^1 \quad g_I = i\tau^1; \quad (\text{A77})$$

$$g_T = \tau^0 \quad g_{P_x} = i\tau^3 \quad g_{P_y} = \tau^0 \quad g_I = \tau^0; \quad (\text{A78})$$

$$g_T = \tau^0 \quad g_{P_x} = \tau^0 \quad g_{P_y} = i\tau^3 \quad g_I = \tau^0; \quad (\text{A79})$$

$$g_T = \tau^0 \quad g_{P_x} = \tau^0 \quad g_{P_y} = \tau^0 \quad g_I = i\tau^3; \quad (\text{A80})$$

$$g_T = i\tau^3 \quad g_{P_x} = i\tau^3 \quad g_{P_y} = \tau^0 \quad g_I = \tau^0; \quad (\text{A81})$$

$$g_T = i\tau^3 \quad g_{P_x} = \tau^0 \quad g_{P_y} = i\tau^3 \quad g_I = \tau^0; \quad (\text{A82})$$

$$g_T = i\tau^3 \quad g_{P_x} = \tau^0 \quad g_{P_y} = \tau^0 \quad g_I = i\tau^3; \quad (\text{A83})$$

$$g_T = i\tau^3 \quad g_{P_x} = i\tau^1 \quad g_{P_y} = \tau^0 \quad g_I = \tau^0; \quad (\text{A84})$$

$$g_T = i\tau^3 \quad g_{P_x} = \tau^0 \quad g_{P_y} = i\tau^1 \quad g_I = \tau^0; \quad (\text{A85})$$

$$g_T = i\tau^3 \quad g_{P_x} = \tau^0 \quad g_{P_y} = \tau^0 \quad g_I = i\tau^1; \quad (\text{A86})$$

$$g_T = \tau^0 \quad g_{P_x} = i\tau^3 \quad g_{P_y} = i\tau^3 \quad g_I = \tau^0; \quad (\text{A87})$$

$$g_T = \tau^0 \quad g_{P_x} = i\tau^3 \quad g_{P_y} = \tau^0 \quad g_I = i\tau^3; \quad (\text{A88})$$

$$g_T = \tau^0 \quad g_{P_x} = \tau^0 \quad g_{P_y} = i\tau^3 \quad g_I = i\tau^3; \quad (\text{A89})$$

$$g_T = i\tau^3 \quad g_{P_x} = i\tau^3 \quad g_{P_y} = i\tau^3 \quad g_I = \tau^0; \quad (\text{A90})$$

$$g_T = i\tau^3 \quad g_{P_x} = i\tau^3 \quad g_{P_y} = \tau^0 \quad g_I = i\tau^3; \quad (\text{A91})$$

$$g_T = i\tau^3 \quad g_{P_x} = \tau^0 \quad g_{P_y} = i\tau^3 \quad g_I = i\tau^3; \quad (\text{A92})$$

$$g_T = i\tau^3 \quad g_{P_x} = i\tau^1 \quad g_{P_y} = i\tau^1 \quad g_I = \tau^0; \quad (\text{A93})$$

$$g_T = i\tau^3 \quad g_{P_x} = i\tau^1 \quad g_{P_y} = i\tau^0 \quad g_I = i\tau^1; \quad (\text{A94})$$

$$g_T = i\tau^3 \quad g_{P_x} = \tau^0 \quad g_{P_y} = i\tau^1 \quad g_I = i\tau^1; \quad (\text{A95})$$

$$g_T = \tau^0 \quad g_{P_x} = i\tau^3 \quad g_{P_y} = i\tau^1 \quad g_I = \tau^0; \quad (\text{A96})$$

$$g_T = \tau^0 \quad g_{P_x} = i\tau^1 \quad g_{P_y} = \tau^0 \quad g_I = i\tau^3; \quad (\text{A97})$$

$$g_T = \tau^0 \quad g_{P_x} = \tau^0 \quad g_{P_y} = i\tau^3 \quad g_I = i\tau^1; \quad (\text{A98})$$

$$g_T = i\tau^3 \quad g_{P_x} = i\tau^3 \quad g_{P_y} = i\tau^1 \quad g_I = \tau^0; \quad (\text{A99})$$

$$g_T = i\tau^3 \quad g_{P_x} = i\tau^1 \quad g_{P_y} = \tau^0 \quad g_I = i\tau^3; \quad (\text{A100})$$

$$g_T = i\tau^3 \quad g_{P_x} = \tau^0 \quad g_{P_y} = i\tau^3 \quad g_I = i\tau^1; \quad (\text{A101})$$

$$g_T = i\tau^3 \quad g_{P_x} = i\tau^1 \quad g_{P_y} = i\tau^3 \quad g_I = \tau^0; \quad (\text{A102})$$

$$g_T = i\tau^3 \quad g_{P_x} = i\tau^3 \quad g_{P_y} = \tau^0 \quad g_I = i\tau^1; \quad (\text{A103})$$

$$g_T = i\tau^3 \quad g_{P_x} = \tau^0 \quad g_{P_y} = i\tau^1 \quad g_I = i\tau^3; \quad (\text{A104})$$

$$g_T = \tau^0 \quad g_{P_x} = i\tau^3 \quad g_{P_y} = i\tau^3 \quad g_I = i\tau^1; \quad (\text{A105})$$

$$g_T = \tau^0 \quad g_{P_x} = i\tau^3 \quad g_{P_y} = i\tau^1 \quad g_I = i\tau^3; \quad (\text{A106})$$

$$g_T = \tau^0 \quad g_{P_x} = i\tau^1 \quad g_{P_y} = i\tau^3 \quad g_I = i\tau^3; \quad (\text{A107})$$

$$g_T = i\tau^3 \quad g_{P_x} = i\tau^3 \quad g_{P_y} = i\tau^3 \quad g_I = i\tau^1; \quad (\text{A108})$$

$$g_T = i\tau^3 \quad g_{P_x} = i\tau^3 \quad g_{P_y} = i\tau^1 \quad g_I = i\tau^3; \quad (\text{A109})$$

$$g_T = i\tau^3 \quad g_{P_x} = i\tau^1 \quad g_{P_y} = i\tau^3 \quad g_I = i\tau^3; \quad (\text{A110})$$

$$g_T = i\tau^3 \quad g_{P_x} = i\tau^3 \quad g_{P_y} = i\tau^1 \quad g_I = i\tau^1; \quad (\text{A111})$$

$$g_T = i\tau^3 \quad g_{P_x} = i\tau^1 \quad g_{P_y} = i\tau^3 \quad g_I = i\tau^1; \quad (\text{A112})$$

$$g_T = i\tau^3 \quad g_{P_x} = i\tau^1 \quad g_{P_y} = i\tau^1 \quad g_I = i\tau^3; \quad (\text{A113})$$

$$g_T = i\tau^3 \quad g_{P_x} = i\tau^1 \quad g_{P_y} = i\tau^1 \quad g_I = i\tau^2; \quad (\text{A114})$$

$$g_T = i\tau^3 \quad g_{P_x} = i\tau^1 \quad g_{P_y} = i\tau^2 \quad g_I = i\tau^1; \quad (\text{A115})$$

$$g_T = i\tau^3 \quad g_{P_x} = i\tau^2 \quad g_{P_y} = i\tau^1 \quad g_I = i\tau^1; \quad (\text{A116})$$

$$g_T = \tau^0 \quad g_{P_x} = i\tau^1 \quad g_{P_y} = i\tau^2 \quad g_I = i\tau^3; \quad (\text{A117})$$

$$g_T = i\tau^3 \quad g_{P_x} = i\tau^1 \quad g_{P_y} = i\tau^2 \quad g_I = i\tau^3; \quad (\text{A118})$$

$$g_T = i\tau^3 \quad g_{P_x} = i\tau^3 \quad g_{P_y} = i\tau^1 \quad g_I = i\tau^2; \quad (\text{A119})$$

$$g_T = i\tau^3 \quad g_{P_x} = i\tau^2 \quad g_{P_y} = i\tau^3 \quad g_I = i\tau^1; \quad (\text{A120})$$

There are 48 different gauge inequivalent choices of g_s . Therefore, the total number of PSGs is $48 \times 2^5 \times 4 = 6144$. However, when $g_T = \tau^0$, to acquire non-vanishing ansatz, η_T must be identical to $2^0 - 1$. Therefore, $15 \times 2^4 \times 4 = 960$ PSGs are killed and the totally number of PSGs reduces to 5184.

2. Ansatzes of the Nearest-Neighbour Spin Coupling Model

In this section we assume that only $u_{i,i+x}$, $u_{i,i+y}$, $u_{i,i+z}$, $u_{i,i-x+z}$, $u_{i,i-y+z}$ and $u_{i,i-x-y+z}$ are non-vanishing. First, an ansatz $u_{i,i+m}$ under $T_x G_x$, $T_y G_y$ and $T_z G_z$ reads

$$u_{i,i+m} = \eta_x^{i_x m_x} \eta_y^{i_y m_y} u_m^l \tau^l, \quad l = 0, 1, 2, 3, \quad (\text{A121})$$

where u_m^i , $i = 1, 2, 3$ is real and u_m^0 is pure imaginary. \mathcal{T} and I further give constraints

$$\eta_t^{m_z} g_T u_m^l \tau^l g_T^{-1} = -u_m^l \tau^l; \quad (\text{A122})$$

$$\eta_I^{m_z} g_I u_m^l \tau^l g_I^{-1} = u_{I(m)}^l \tau^l. \quad (\text{A123})$$

Using $u_{I(m)} = u_{-m} = u_m^\dagger$, we can conclude that when

$$\eta_t = 1, \eta_I = 1, g_T = i\tau^3, \text{ and } g_I = i\tau^3, \quad (\text{A124})$$

all u_m vanish. This kills $10 \times 2^3 \times 4 = 320$ PSGs and the totally number of PSGs is $5184 - 320 = 4864$. When

$$\eta_t \eta_I = -1, g_T = i\tau^3, g_I = i\tau^{1,2} \text{ or } \tau^0, \quad (\text{A125})$$

all u_m^l vanish for odd m_z , namely only $u_{i,i+x}$ and $u_{i,i+y}$ remain non-zero. These ansatzes degenerate to describe spin liquids in a rectangular lattice in 2D plane, which is irrelevant to us. There is another similar case. When $G_x = (-)^{i_z} \tau^0$, G_{P_x} will give the constraint

$$\left(\cos\left(\frac{\pi}{2} m_z\right) + (-)^{i_z} \sin\left(\frac{\pi}{2} m_z\right) \right) \cdot \eta_p^{m_y} g_{P_x} u_m^l \tau^l g_{P_x}^{-1} = u_{P_x(m)}^l \tau^l. \quad (\text{A126})$$

For odd m_z , *l.h.s.* is a function of i_z while *r.h.s.* is not, which indicates that all the u_m^l for odd m_z must vanish to satisfy the equation. As indicated in the previous argument, we do not take consideration of these ansatzes. Therefore, only $G_x(i) = G_y(i) = \tau^0$ case will be under consideration. The number of PSGs left is $(4864 - (9 + 14) \times 2^3 \times 4) \div 4 = 1032$.

When $G_x(i) = G_y(i) = \tau^0$, P_x and P_y give constraints on ansatzes

$$g_{P_x} u_x^l \tau^l g_{P_x}^{-1} = u_x^l \tau^l; \quad (\text{A127})$$

$$\eta_p g_{P_x} u_y^l \tau^l g_{P_x}^{-1} = u_y^l \tau^l; \quad (\text{A128})$$

$$\eta_{5px} g_{P_x} u_z^l \tau^l g_{P_x}^{-1} = u_{-x+z}^l \tau^l; \quad (\text{A129})$$

$$\eta_p \eta_{5px} g_{P_x} u_{-y+z}^l \tau^l g_{P_x}^{-1} = u_{-x-y+z}^l \tau^l; \quad (\text{A130})$$

$$\eta_p g_{P_y} u_x^l \tau^l g_{P_y}^{-1} = u_x^l \tau^l; \quad (\text{A131})$$

$$g_{P_y} u_y^l \tau^l g_{P_y}^{-1} = u_y^l \tau^l; \quad (\text{A132})$$

$$\eta_{5py} g_{P_y} u_z^l \tau^l g_{P_y}^{-1} = u_{-y+z}^l \tau^l; \quad (\text{A133})$$

$$\eta_p \eta_{5py} g_{P_y} u_{-x+z}^l \tau^l g_{P_y}^{-1} = u_{-x-y+z}^l \tau^l. \quad (\text{A134})$$

These equations determine the constraints of ansatzes in numerical calculation. Two of the constraints are employed. One is the periodic condition, that the periodicity of all the ansatzes is 1, and the other is the sector condition, that the ansatzes satisfy

$$u_z = s_x u_{-x+z} = s_y u_{-y+z} = s_{xy} u_{-x-y+z}, \quad (\text{A135})$$

with $s_x, s_y, s_{xy} = \pm 1$. According to numerical results, there are at most 311 inequivalent ansatzes.

Appendix B: Numerical Method and Data for Strong Coupling Case

Differential evolution (DE), originally developed by Storn and Price⁴¹, is a meta-heuristic algorithm that globally optimizes a given objective function in an iterative manner. Usually the objective function is treated as a black box and no assumptions are needed. For example, unlike traditional gradient decent, conjugate gradient and quasi-Newton methods, derivatives are not needed. Evaluation of derivatives of mean-field energy defined previously is time-consuming for which DE is suitable. Besides, another algorithm, the Nelder-Mead method is also tested but doesn't perform as good as DE.

DE works with a group (called population) of solution candidates (called agents), which is initialized randomly. In each iterative step, a certain agent is selected and a new agent is generated from this agent and two other randomly selected agents in a random, linear way. If the new agent is better than the old agent, the old agent is replaced by the new one. If not, the trial agent is simply discarded. This procedure continues until some certain accuracy is reached.

In this paper, DE is used to optimize the mean-field energy with respect to ansatzes. Constrained by PSG's, number of optimizing variables is restricted to be 12. The number of agents is set to be 120, 10 times the number of variables, with differential weight being 0.9 and cross over probability being 0.5.

1. Fourier Transformation of the Mean Field Hamiltonian

The mean field Hamiltonian reads

$$H_{MF} = H_{MF}^f + H_{MF}^b \quad (\text{B1})$$

with

$$H_{MF}^f = \frac{3}{8} \sum_{\vec{r}} \sum_{\alpha} [\psi_{\alpha_1}^\dagger(\vec{r}) U_{\alpha} \psi_{\alpha_2}(\vec{r}) + \psi_{\alpha_2}^\dagger(\vec{r}) U_{\alpha}^\dagger \psi_{\alpha_1}(\vec{r})] \quad (\text{B2})$$

and

$$H_{MF}^b = \frac{t}{2} \sum_{\vec{r}} \sum_{\alpha} [b_{\alpha_1}^\dagger(\vec{r}) U_{\alpha} b_{\alpha_2}(\vec{r}) + b_{\alpha_2}^\dagger(\vec{r}) U_{\alpha}^\dagger b_{\alpha_1}(\vec{r})] \quad (\text{B3})$$

Here superscripts f and b mean fermion and boson respectively. \vec{r} refers to the coordinate of one certain super-cell. α refers to the index of one certain bond in a cell. α_1 is index of the first end of bond α , α_2 is the other end. U_{α} is a 2×2 matrix containing various u_{ij} so that above formulas are consistent with equation 5. In this holon-condensed case, bosons are treated as scalars.

Only derivation of Fourier-transformed form for the fermion Hamiltonian is shown in details. The Fourier-transformed form of the boson Hamiltonian can be obtained by just replacing ψ with b since commutation relations are not included in derivation.

Take substitutions

$$\psi_{\alpha_1}(\vec{r}) = \frac{1}{\sqrt{N}} \sum_{\vec{k}} \psi_{\alpha_1}(\vec{k}) e^{i\vec{k} \cdot (\vec{r} + \vec{l}_{\alpha_1})} \quad (\text{B4})$$

and

$$\psi_{\alpha_2}(\vec{r}) = \frac{1}{\sqrt{N}} \sum_{\vec{k}} \psi_{\alpha_2}(\vec{k}) e^{i\vec{k} \cdot (\vec{r} + \vec{l}_{\alpha_2})}, \quad (\text{B5})$$

we further have

$$H_{MF}^f = \frac{3}{8} \sum_{\vec{k}} \sum_{\alpha} [\psi_{\alpha_1}^\dagger(\vec{k}) U_{\alpha} e^{i\vec{k} \cdot (\vec{l}_{\alpha_2} - \vec{l}_{\alpha_1})} \psi_{\alpha_2}(\vec{k}) + \psi_{\alpha_2}^\dagger(\vec{k}) U_{\alpha}^\dagger e^{-i\vec{k} \cdot (\vec{l}_{\alpha_2} - \vec{l}_{\alpha_1})} \psi_{\alpha_1}(\vec{k})]. \quad (\text{B6})$$

It should be noted that this Hamiltonian is block-diagonalized with respect to \vec{k} . So we can calculate eigenvalues and eigenvectors of each block-matrix individually to reduce calculation workload.

2. Evaluation of the Energy

$$\begin{aligned} \mathcal{H}_{MF}^b = & \frac{t}{2} \sum_{\vec{k}} \sum_{\alpha} [b_{\alpha 1}^{\dagger}(\vec{k}) U_{\alpha} e^{i\vec{k} \cdot (\vec{l}_{\alpha 2} - \vec{l}_{\alpha 1})} b_{\alpha 2}(\vec{k}) \\ & + b_{\alpha 2}^{\dagger}(\vec{k}) U_{\alpha}^{\dagger} e^{-i\vec{k} \cdot (\vec{l}_{\alpha 2} - \vec{l}_{\alpha 1})} b_{\alpha 1}(\vec{k})]. \end{aligned} \quad (\text{B7})$$

These two equations can be rephrased in matrix form:

$$H_{MF}^f = \sum_{\vec{k}} \psi^{\dagger}(\vec{k}) Q_{MF}^f(\vec{k}) \psi(\vec{k}) \quad (\text{B8})$$

with

$$\psi(\vec{k}) = \begin{pmatrix} \psi_{1,\uparrow}(\vec{k}) \\ \psi_{2,\uparrow}(\vec{k}) \\ \vdots \\ \psi_{N_{site},\uparrow}(\vec{k}) \\ \psi_{1,\downarrow}(\vec{k}) \\ \vdots \\ \psi_{N_{site},\downarrow}(\vec{k}) \end{pmatrix}. \quad (\text{B9})$$

Here N_{site} means the number of sites in one unit cell. The Q_{MF}^f can be diagonalized as

$$Q_{MF}^f(\vec{k}) = S^f(\vec{k}) D^f(\vec{k}) S^{f\dagger}(\vec{k}). \quad (\text{B10})$$

Denote $\phi(\vec{k}) = S^{f\dagger}(\vec{k}) \psi(\vec{k})$, we further have

$$H_{MF}^f = \sum_{\vec{k}} \sum_{i=1}^{2N_{site}} \lambda_i^f(\vec{k}) \phi_i^{\dagger}(\vec{k}) \phi_i(\vec{k}). \quad (\text{B11})$$

To obtain energy of the original Hamiltonian, we need to evaluate the average $\langle \psi_i^{\dagger}(\vec{k}_1) \psi_j(\vec{k}_2) \rangle_0$. The subscript 0 means that average is taken in a Gaussian level. These two averages can be expressed as

$$\langle \psi_i^{\dagger}(\vec{k}_1) \psi_j(\vec{k}_2) \rangle_0 = \delta_{\vec{k}_1, \vec{k}_2} \sum_{l=1}^{2N_{site}} S_{il}^{f*} S_{jl}^f \langle \phi_l^{\dagger}(\vec{k}_1) \phi_l(\vec{k}_1) \rangle_0, \quad (\text{B12})$$

where

$$\langle \phi_l^{\dagger}(\vec{k}) \phi_l(\vec{k}) \rangle_0 = \begin{cases} 0, & \lambda_l^f(\vec{k}) > 0 \\ 1, & \lambda_l^f(\vec{k}) < 0. \end{cases} \quad (\text{B13})$$

For simplicity, we define several functions:

$$n_f(i, s) = \sum_{\vec{k}} \langle \psi_{i,s}^{\dagger}(\vec{k}) \psi_{i,s}(\vec{k}) \rangle_0, \quad (\text{B14})$$

$$n_b(i, s) = \sum_{\vec{k}} b_{i,s}^{\dagger}(\vec{k}) b_{i,s}(\vec{k}), \quad (\text{B15})$$

$$O_f(\alpha, s_1, s_2) = \sum_{\vec{k}} e^{i\vec{k} \cdot (\vec{l}_{\alpha 2} - \vec{l}_{\alpha 1})} \langle \psi_{\alpha 1, s_1}^{\dagger}(\vec{k}) \psi_{\alpha 2, s_2}(\vec{k}) \rangle_0, \quad (\text{B16})$$

$$O_b(\alpha, s_1, s_2) = \sum_{\vec{k}} e^{i\vec{k} \cdot (\vec{l}_{\alpha 2} - \vec{l}_{\alpha 1})} b_{\alpha 1, s_1}^{\dagger}(\vec{k}) b_{\alpha 2, s_2}(\vec{k}). \quad (\text{B17})$$

Here i is the site index in one super-cell, s , s_1 and s_2 can be \uparrow or \downarrow .

With assistance with definitions above, energy of the original Hamiltonian can be expressed as

$$\langle H \rangle_0 = \langle H_1 \rangle_0 - t \langle H_2 \rangle_0, \quad (\text{B18})$$

$$\begin{aligned} \langle H_1 \rangle_0 = \sum_{\alpha} [& \frac{N_{cell}}{4} - \frac{1}{4} n_f(\alpha_1, \uparrow) - \frac{1}{4} n_f(\alpha_1, \downarrow) \\ & - \frac{1}{4} n_f(\alpha_2, \downarrow) - \frac{1}{4} n_f(\alpha_2, \downarrow) \\ & - \frac{1}{2N_{cell}} O_f(\alpha, \downarrow, \uparrow) O_f(\alpha, \uparrow, \downarrow) \\ & + \frac{1}{2N_{cell}} O_f(\alpha, \uparrow, \uparrow) O_f(\alpha, \downarrow, \downarrow) \\ & - \frac{1}{2N_{cell}} O_f^*(\alpha, \downarrow, \uparrow) O_f^*(\alpha, \uparrow, \downarrow) \\ & + \frac{1}{2N_{cell}} O_f^*(\alpha, \uparrow, \uparrow) O_f^*(\alpha, \downarrow, \downarrow) \\ & - \frac{1}{4N_{cell}} O_f^*(\alpha, \uparrow, \uparrow) O_f(\alpha, \uparrow, \uparrow) \\ & + \frac{1}{4N_{cell}} n_f(\alpha_1, \uparrow) n_f(\alpha_2, \uparrow) \\ & - \frac{1}{4N_{cell}} O_f^*(\alpha, \uparrow, \downarrow) O_f(\alpha, \uparrow, \downarrow) \\ & + \frac{1}{4N_{cell}} n_f(\alpha_1, \uparrow) n_f(\alpha_2, \downarrow) \\ & - \frac{1}{4N_{cell}} O_f^*(\alpha, \downarrow, \uparrow) O_f(\alpha, \downarrow, \uparrow) \\ & + \frac{1}{4N_{cell}} n_f(\alpha_1, \downarrow) n_f(\alpha_2, \uparrow) \\ & - \frac{1}{4N_{cell}} O_f^*(\alpha, \downarrow, \downarrow) O_f(\alpha, \downarrow, \downarrow) \\ & + \frac{1}{4N_{cell}} n_f(\alpha_1, \downarrow) n_f(\alpha_2, \downarrow)], \end{aligned} \quad (\text{B19})$$

and

$$\begin{aligned}
\langle H_2 \rangle_0 = \frac{1}{2N_{cell}} \sum_{\alpha} [& O_b(\alpha, \uparrow, \downarrow) O_f(\alpha, \downarrow, \uparrow) \\
& + O_b(\alpha, \downarrow, \uparrow) O_f(\alpha, \uparrow, \downarrow) \\
& - O_b(\alpha, \uparrow, \uparrow) O_f(\alpha, \downarrow, \downarrow) \\
& - O_b(\alpha, \downarrow, \downarrow) O_f(\alpha, \uparrow, \uparrow) \\
& + O_b^*(\alpha, \uparrow, \downarrow) O_f^*(\alpha, \downarrow, \uparrow) \\
& + O_b^*(\alpha, \downarrow, \uparrow) O_f^*(\alpha, \uparrow, \downarrow) \\
& - O_b^*(\alpha, \uparrow, \uparrow) O_f^*(\alpha, \downarrow, \downarrow) \\
& - O_b^*(\alpha, \downarrow, \downarrow) O_f^*(\alpha, \uparrow, \uparrow) \\
& + O_b(\alpha, \uparrow, \uparrow) O_f^*(\alpha, \uparrow, \uparrow) \\
& + O_b(\alpha, \uparrow, \downarrow) O_f^*(\alpha, \uparrow, \downarrow) \\
& + O_b(\alpha, \downarrow, \uparrow) O_f^*(\alpha, \downarrow, \uparrow) \\
& + O_b(\alpha, \downarrow, \downarrow) O_f^*(\alpha, \downarrow, \downarrow) \\
& + O_b^*(\alpha, \uparrow, \uparrow) O_f(\alpha, \uparrow, \uparrow) \\
& + O_b^*(\alpha, \uparrow, \downarrow) O_f(\alpha, \uparrow, \downarrow) \\
& + O_b^*(\alpha, \downarrow, \uparrow) O_f(\alpha, \downarrow, \uparrow) \\
& + O_b^*(\alpha, \downarrow, \downarrow) O_f(\alpha, \downarrow, \downarrow)]. \quad (B20)
\end{aligned}$$

Appendix C: Construction of the Interaction Hamiltonian in Weak Coupling Limit

A generic interaction term reads (spin indices neglected)²³

$$\begin{aligned}
H' = \int \prod_a \frac{k_a}{2\pi} \sum_{P_a, i_a} \delta(Q) V(P_a, i_a, k_a) \\
\psi_{i_1}^{P_1 \dagger}(k_1) \psi_{i_2}^{P_2 \dagger}(k_2) \psi_{i_3}^{P_3}(k_3) \psi_{i_4}^{P_4}(k_4), \quad (C1)
\end{aligned}$$

where $P = 1(-1)$ for R(L). The constraint of momentum conservation

$$\begin{aligned}
0 = Q = -P_1 k_{Fi_1} - P_2 k_{Fi_2} + P_3 k_{Fi_3} + P_4 k_{Fi_4} \\
- k_1 - k_2 + k_3 + k_4. \quad (C2)
\end{aligned}$$

As the momentum of chiral fermions (k_i) are much smaller than Fermi vectors (k_{Fi}), the momentum conservation is reduced to

$$-P_1 k_{Fi_1} - P_2 k_{Fi_2} + P_3 k_{Fi_3} + P_4 k_{Fi_4} = 0. \quad (C3)$$

Therefore, only two types of interactions are allowed. The first one is intra-band scattering $\psi_i^{R\dagger} \psi_j^{L\dagger} \psi_j^L \psi_i^R$ and the second one is inter-band scattering $\psi_i^{R\dagger} \psi_i^{L\dagger} \psi_{3-i}^L \psi_{3-i}^R$. The purely chiral terms like $\psi_i^{R\dagger} \psi_j^{R\dagger} \psi_j^R \psi_i^R$ do not generate renormalization at leading order²³ and thus are neglected. When spin is included, we define charge and spin current

$$T_{ij} = \sum_s \psi_{i,s}^\dagger \psi_{j,s}, \quad (C4)$$

$$\vec{T}_{ij} = \frac{1}{2} \sum_{s,s'} \psi_{i,s}^\dagger \vec{\sigma}_{ss'} \psi_{j,s'}, \quad (C5)$$

and the interaction Hamiltonian density in real space can be written as

$$\begin{aligned}
\mathcal{H}' = f_{ij}^\rho T_{ii}^R T_{jj}^L - f_{ij}^\sigma \vec{T}_{ii}^R \cdot \vec{T}_{jj}^L \\
+ f_{ii}^{\prime\rho} T_{i,3-i}^R T_{i,3-i}^L - f_{ii}^{\prime\sigma} \vec{T}_{i,3-i}^R \cdot \vec{T}_{ij}^L, \quad (C6)
\end{aligned}$$

Appendix D: Derivation of RG Equations

Define $z_i = v_i \tau - ix$. Determined by the operator product expansion (OPE) in terms of chiral fermions

$$\psi_{i,s}^R(x, \tau) \psi_{j,s'}^{R\dagger}(0, 0) \sim \frac{\delta_{ij} \delta_{ss'}}{2\pi z_i}, \quad (D1)$$

$$\psi_{i,s}^L(x, \tau) \psi_{j,s'}^{L\dagger}(0, 0) \sim \frac{\delta_{ij} \delta_{ss'}}{2\pi z_i^*}, \quad (D2)$$

the current algebra reads²³

$$T_{ij}^R(x, \tau) T_{lm}^R(0, 0) \sim \frac{\delta_{il}}{2\pi z_j} T_{jm}^R - \frac{\delta_{jm}}{2\pi z_i} T_{il}^R, \quad (D3)$$

$$\begin{aligned}
T_{ij}^{Ra}(x, \tau) T_{lm}^{Rb}(0, 0) \sim \frac{\delta_{ab}}{4} \left(\frac{\delta_{il}}{2\pi z_j} T_{jm}^R - \frac{\delta_{jm}}{2\pi z_i} T_{il}^R \right) \\
+ \frac{i\epsilon_{abc}}{2} \left(\frac{\delta_{il}}{2\pi z_j} T_{jm}^{Rc} + \frac{\delta_{jm}}{2\pi z_i} T_{il}^{Rc} \right), \quad (D4)
\end{aligned}$$

$$T_{ij}^{Ra}(x, \tau) T_{lm}^R(0, 0) \sim \frac{\delta_{il}}{2\pi z_j} T_{jm}^{Ra} - \frac{\delta_{jm}}{2\pi z_i} T_{il}^{Ra}, \quad (D5)$$

where T^{Ra} is the components of the vector current \vec{T}^R . For T^L , the current algebra is the same, except $z_i \rightarrow z_i^*$. Employing the standard method³⁵ and using the current algebra above, we obtain the RG equations

$$\dot{f}_{ii}^\rho = -\frac{16(f_{ii}^{\prime\rho})^2 + 3(f_{ii}^{\prime\sigma})^2}{32\pi v_i}, \quad (D6)$$

$$\dot{f}_{ii}^\sigma = -\frac{2(f_{ii}^\sigma)^2 + 4f_{ii}^{\prime\rho} f_{ii}^{\prime\sigma} + (f_{ii}^{\prime\sigma})^2}{4\pi v_i}, \quad (D7)$$

$$\dot{f}_{i,3-i}^\rho = \frac{16(f_{ii}^{\prime\rho})^2 + 3(f_{ii}^{\prime\sigma})^2}{16\pi(v_i + v_{3-i})}, \quad (D8)$$

$$\dot{f}_{i,3-i}^\sigma = \frac{2(f_{i,3-i}^\sigma)^2 + 4f_{ii}^{\prime\rho} f_{ii}^{\prime\sigma} - (f_{ii}^{\prime\sigma})^2}{2\pi(v_i + v_{3-i})}, \quad (D9)$$

$$\begin{aligned}
\dot{f}_{ii}^{\prime\rho} = \frac{16f_{ij}^\rho f_{ii}^{\prime\rho} + 3f_{ij}^\sigma f_{ii}^{\prime\sigma}}{8\pi(v_i + v_{3-i})} \\
- \sum_i \frac{16f_{ii}^\rho f_{ii}^{\prime\rho} + 3f_{ii}^\sigma f_{ii}^{\prime\sigma}}{32\pi v_i}, \quad (D10)
\end{aligned}$$

$$\begin{aligned}
\dot{f}_{ii}^{\prime\sigma} = \frac{2f_{ij}^\rho f_{ii}^{\prime\sigma} + 2f_{ij}^\sigma f_{ii}^{\prime\rho} - f_{ij}^\sigma f_{ii}^{\prime\sigma}}{\pi(v_i + v_{3-i})} \\
- \sum_i \frac{2f_{ii}^\rho f_{ii}^{\prime\sigma} + 2f_{ii}^\sigma f_{ii}^{\prime\rho} + f_{ii}^\sigma f_{ii}^{\prime\sigma}}{4\pi v_i}. \quad (D11)
\end{aligned}$$

Symmetries of the coupling constants are employed in the derivation of the equations above. The initial value

of these coupling constants are

$$f_{ij,0}^\rho = \frac{1}{4}f_{ij}^\sigma = J'(1 - (-1)^{i+j} \cos(\frac{k_{Fi} + k_{Fj}}{2})) + \frac{1}{2}J(1 - \cos(k_{Fi} + k_{Fj})) + \delta_{ij}J_y, \quad (\text{D12})$$

$$f_{ii,0}^{\prime\rho} = \frac{1}{4}f_{ii}^{\prime\sigma} = J \sin(k_{F1}) \sin(k_{F2}) - 2J' \sin(\frac{k_{F1}}{2}) \sin(\frac{k_{F2}}{2}) - J_y. \quad (\text{D13})$$

The RG flows are calculated numerically.

Appendix E: Bosonization Dictionary³⁵

The bosonization dictionary³⁵ reads

$$\psi_{i,s}^{R/L} \sim \eta_{i,s} e^{i\sqrt{4\pi}\phi_{i,s}^{R/L}}, \quad (\text{E1})$$

where the chiral boson fields satisfy commutation relation²³

$$[\phi_{i,s}^R(x), \phi_{i',s'}^R(y)] = -[\phi_{i,s}^L(x), \phi_{i',s'}^L(y)] = \frac{i}{4} \text{sgn}(x - y) \delta_{ii'} \delta_{ss'}, \quad (\text{E2})$$

$$[\phi_{i,s}^R(x), \phi_{i',s'}^L(y)] = \frac{i}{4} \delta_{ii'} \delta_{ss'}, \quad (\text{E3})$$

and η_s are Klein factors satisfying $\{\eta_{i,s}, \eta_{i',s'}\} = 2\delta_{ii'} \delta_{ss'}$. To describe spin and charge modes, we further define

$$\phi_{i,\rho} = \frac{1}{\sqrt{2}}(\phi_{i,\uparrow}^R + \phi_{i,\downarrow}^R + \phi_{i,\uparrow}^L + \phi_{i,\downarrow}^L), \quad (\text{E4})$$

$$\theta_{i,\rho} = \frac{1}{\sqrt{2}}(\phi_{i,\uparrow}^R + \phi_{i,\downarrow}^R - \phi_{i,\uparrow}^L - \phi_{i,\downarrow}^L), \quad (\text{E5})$$

$$\phi_{i,\sigma} = \frac{1}{\sqrt{2}}(\phi_{i,\uparrow}^R - \phi_{i,\downarrow}^R + \phi_{i,\uparrow}^L - \phi_{i,\downarrow}^L), \quad (\text{E6})$$

$$\theta_{i,\sigma} = \frac{1}{\sqrt{2}}(\phi_{i,\uparrow}^R - \phi_{i,\downarrow}^R - \phi_{i,\uparrow}^L + \phi_{i,\downarrow}^L), \quad (\text{E7})$$

where subscript ρ represents charge mode and σ represents spin mode, respectively.

-
- * These two authors contribute equally to this work.
- ¹ E. Dagotto, Reviews of Modern Physics **66**, 763 (1994).
 - ² A. J. Leggett, Nature Physics **2**, 134 (2006).
 - ³ J. G. Bednorz and K. A. Müller, Zeitschrift für Physik B Condensed Matter **64**, 189 (1986).
 - ⁴ A. Schilling, M. Cantoni, J. D. Guo, and H. R. Ott, Nature **363**, 56 (1993).
 - ⁵ L. Gao, Y. Y. Xue, F. Chen, Q. Xiong, R. L. Meng, D. Ramirez, C. W. Chu, J. H. Eggert, and H. K. Mao, Physical Review B **50**, 4260 (1994).
 - ⁶ S. Chakravarty, A. Sudbø, P. Anderson, and S. Strong, Science **261**, 337 (1993).
 - ⁷ J. R. Kirtley, C. C. Tsuei, Ariando, C. J. M. Verwijs, S. Harkema, and H. Hilgenkamp, Nature Physics **2**, 190 (2006).
 - ⁸ C. C. Tsuei, Physical Review Letters **73**, 593 (1994).
 - ⁹ C. C. Tsuei, J. R. Kirtley, Z. F. Ren, J. H. Wang, H. Raffy, and Z. Z. Li, Nature **387**, 481 (1997).
 - ¹⁰ D. Matsunaka, E. T. Rodulfo, and H. Kasai, Solid State Communications **134**, 355 (2005).
 - ¹¹ W. Li, J. Zhao, L. Cao, Z. Hu, Q. Huang, X. Wang, Y. Liu, G. Zhao, J. Zhang, Q. Liu, R. Yu, Y. Long, H. Wu, H. Lin, C. Chen, Z. Li, Z. Gong, Z. Guguchia, J. Kim, G. Stewart, Y. Uemura, S. Uchida, and C. Jin, PNAS; Proceedings of the National Academy of Sciences **116**, 12156 (2019).
 - ¹² W. M. Li, J. F. Zhao, L. P. Cao, Z. Hu, Q. Z. Huang, X. C. Wang, R. Z. Yu, Y. W. Long, H. Wu, H. J. Lin, and et al., Journal of Superconductivity and Novel Magnetism **33**, 81 (2019).
 - ¹³ T. Maier, T. Berlijn, and D. J. Scalapino, Physical Review B **99** (2019), 10.1103/PhysRevB.99.224515.
 - ¹⁴ Z. Wang, S. Zhou, W. Chen, and F.-C. Zhang, Physical Review B **101** (2020), 10.1103/PhysRevB.101.180509.
 - ¹⁵ C. Le, K. Jiang, Y. Li, S. Qin, Z. Wang, F. Zhang, and J. Hu, (2019), 1909.12620.
 - ¹⁶ Y. Ni, Y.-M. Quan, J. Liu, Y. Song, and L.-J. Zou, (2019), 1912.10580.
 - ¹⁷ K. Yamazaki, M. Ochi, D. Ogura, K. Kuroki, H. Eisaki, S. Uchida, and H. Aoki, (2020), 2003.04015.
 - ¹⁸ Q. Zhang, K. Jiang, Y. Gu, and J. Hu, SCIENCE CHINA Physics, Mechanics and Astronomy **63** (2019), 10.1007/s11433-019-1495-3, 1910.10904.
 - ¹⁹ K. Liu, Z.-Y. Lu, and T. Xiang, Physical Review Materials **3** (2019), 10.1103/PhysRevMaterials.3.044802.
 - ²⁰ X.-G. Wen, Physical Review B **65** (2002), 65.165113.
 - ²¹ Y. Zhou and X.-G. Wen, cond-mat/0210662.
 - ²² P. A. Lee, N. Nagaosa, and X.-G. Wen, Reviews of Modern Physics **78**, 17 (2006).
 - ²³ H.-H. Lin, L. Balents, and M. P. A. Fisher, Physical Review B **56**, 6569 (1997).
 - ²⁴ T. Tonegawa, K. Okamoto, T. Hikihara, and T. Sakai, Journal of Physics: Conference Series **828**, 012003 (2017).
 - ²⁵ Q. Luo, S. Hu, J. Zhao, A. Metavitsiadis, S. Eggert, and X. Wang, Physical Review B **97** (2018), 10.1103/physrevb.97.214433.
 - ²⁶ G. Giri, Physical Review B **95** (2017), 10.1103/PhysRevB.95.224408.
 - ²⁷ D. Scalapino, Physical Review B **58**, 443 (1998).
 - ²⁸ C. Wu, Physical Review B **68** (2003), 10.1103/PhysRevB.68.115104.
 - ²⁹ L. Balents and M. P. A. Fisher, Physical Review B **53**, 12133 (1996).
 - ³⁰ D. G. Shelton, Physical Review B **58**, 6818 (1998).
 - ³¹ E. Orignac, Physical Review B **56**, 7167 (1997).
 - ³² H. J. Schulz, Physical Review B **53**, R2959 (1996).
 - ³³ M. Fabrizio, Physical Review B **48**, 15838 (1993).

- ³⁴ C. M. Varma, Physical Review B **32**, 7399 (1985).
- ³⁵ E. Fradkin, Field Theories of Condensed Matter Physics (Cambridge University Press, 2013).
- ³⁶ P. W. Anderson, Phys. Rev. Lett. **3**, 325 (1959).
- ³⁷ A. V. Balatsky, Reviews of Modern Physics **78**, 373 (2006).
- ³⁸ D. J. V. Harlingen, Reviews of Modern Physics **67**, 515 (1995).
- ³⁹ C. C. Tsuei, Reviews of Modern Physics **72**, 969 (2000).
- ⁴⁰ A. Damascelli, Reviews of Modern Physics **75**, 473 (2003).
- ⁴¹ R. Storn and K. Price, Journal of Global Optimization **11**, 341 (1997).